Infrared Spectroscopy of the *syn*-Methyl-Substituted Criegee Intermediate: A Combined Experimental and Theoretical Study

Meijun Zou[a,†], Yarra Hassan[b,†], Tarun Kumar Roy[a], Anne B. McCoy[*,b] and Marsha I. Lester[*,a]

[a] Department of Chemistry, University of Pennsylvania, Philadelphia, PA 19104-6323, USA
[b] Department of Chemistry, University of Washington, Seattle, WA 98195-1700, USA

Abstract

An IR-VUV ion-dip spectroscopy method is utilized to examine the IR spectrum of acetaldehyde oxide (CH_3CHOO) in the overtone CH stretch ($2\nu_{CH}$) spectral region. IR activation creates a depletion of the ground state population that reduces the VUV photoionization signal on the parent mass channel. IR activation of the more stable and populated *syn*-CH_3CHOO conformer results in rapid unimolecular decay to OH + vinoxy products and makes the most significant contribution to the observed spectrum. The resultant IR-VUV ion dip spectrum of CH_3CHOO is similar to that obtained previously for *syn*-CH_3CHOO using IR action spectroscopy with UV laser-induced fluorescence detection of OH products. The prominent IR features at 5984 and 6081 cm^{-1} are also observed using UV+VUV photoionization of OH products. Complementary theoretical calculations utilizing a general implementation of second order vibrational perturbation theory provide new insights on the vibrational transitions that give rise to the experimental spectrum in the overtone CH stretch region. The introduction of physically motivated small shifts of the harmonic frequencies yields remarkably improved agreement between experiment and theory in the overtone CH stretch region. The prominent features are assigned as highly mixed states with contributions from two quanta of CH stretch and/or a combination of CH stretch with an overtone in mode 4. The generality of this approach is demonstrated by applying it to three different levels of electronic structure theory/basis sets, all of which provide spectra that are virtually indistinguishable despite showing large deviations prior to introducing the shifts to the harmonic frequencies.

† Equal contributions.
* Corresponding author emails: abmccoy@uw.edu, milester@sas.upenn.edu

Introduction

Criegee intermediates are transient reaction intermediates with zwitterionic carbonyl oxide character ($R_1R_2C{=}O^+O^-$) formed in the ozonolysis of alkenes, the most abundant volatile organic compounds (VOCs) emitted into the atmosphere after methane.[1, 2] The Criegee intermediates are typically formed with significant excess energy (ca. 50 kcal mol^{-1}) and can undergo unimolecular decay promptly or after thermalization, leading to hydroxyl (OH) radicals and other products.[3, 4] Alternatively, the Criegee intermediates can react with water vapor or trace atmospheric gases, which can lead to secondary organic aerosol formation.[5-7] This study reexamines the infrared spectrum of the acetaldehyde oxide (CH_3CHOO) Criegee intermediate, both experimentally and theoretically, in the overtone CH stretch ($2\nu_{CH}$) region. This spectral region offers relatively strong transitions for spectroscopic identification of the Criegee intermediates at energies in the vicinity of the transition state (TS) barrier(s) leading to unimolecular decay.

The CH_3CHOO Criegee intermediate has two distinct conformational forms, *syn* and *anti*, in which the terminal oxygen points toward or away from the methyl group as shown in Figure 1. The *syn* conformer is more stable by ca. 3 kcal mol^{-1} due to an intramolecular hydrogen bonding interaction between the methyl group and terminal oxygen. The two conformers of stabilized CH_3CHOO do not interconvert due to the high isomerization barrier (ca. 38 kcal mol^{-1})[8] associated with internal rotation about the C=O bond. Most recent laboratory studies generate CH_3CHOO through an alternate synthetic approach in which a diiodo ethane precursor (CH_3CHI_2) is photolyzed at 248 nm (or 351 nm), generating an internally hot CH_3CHI radical, which subsequently reacts with O_2 to displace the remaining I atom and form CH_3CHOO. The *syn* and *anti* conformers of CH_3CHOO are rapidly thermalized or jet-cooled prior to VUV photoionization,[9] UV absorption,[10-13] IR spectroscopy,[4, 14-18] or FTMW studies.[19, 20] Prior studies have also examined the conformer-dependent bimolecular reactions of *syn*- and *anti*-CH_3CHOO with water vapor and trace atmospheric gases.[8, 9, 11, 15, 21-25]

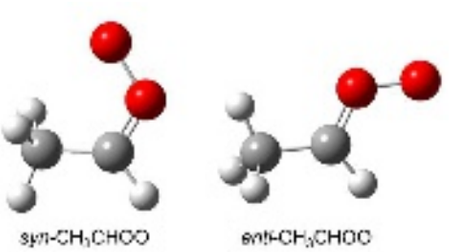

Figure 1. Structures of the *syn* (left) and *anti* (right) conformers of CH_3CHOO with the terminal oxygen pointing toward or away from the methyl group, respectively.

Earlier work in this laboratory examined the IR spectroscopy and unimolecular decay dynamics of *syn*-CH_3CHOO upon vibrational activation in the overtone CH stretch ($2\nu_{CH}$),[4, 14, 17] combination band ($\nu_{CH} + \nu_j$),[16] and fundamental CH stretch (ν_{CH})[18] regions under jet-cooled and isolated conditions. In each

case, IR action spectra were recorded with UV laser-induced fluorescence (LIF) detection of OH products resulting from unimolecular decay. Most of the above studies were supported by calculations of the vibrational spectra, typically performed using second order vibrational perturbation theory (VPT2). While the VPT2 calculations did an excellent job of reproducing the measured spectrum in the fundamental CH stretch region at ca. 3000 cm^{-1},[18] spectral assignments were not rigorous at higher energies. Indeed, large differences were noted in the region that reflected excitation of two quanta in the CH stretching vibrations. At these energies, the density of vibrational states is much larger, leading to strongly coupled states that are close in energy. In these situations, small discrepancies in the vibrational frequencies of the CH stretches can lead to large changes in the overall spectral envelope.[26-28] Additionally, the states with two quanta in the CH stretching vibrations are expected to be coupled to states that involve three or four quanta of excitation. In studying this spectral region, we exploit the flexibility of a recently developed implementation of vibrational perturbation theory, PyVibPT*n*,[29, 30] which is based on the development of perturbation theory originally described by Sakurai and Kato.[31, 32] This code has been used in studies of several similarly sized and larger molecules, e.g. protonated ethene, the vinoxide anion and a hydroperoxyalkyl radical, with good success.[28, 33, 34] In this work, we explore how we can incorporate semi-empirical corrections to the harmonic frequencies to improve the agreement between experiment and calculation using this approach.

The unimolecular decay of *syn*-CH_3CHOO proceeds by 1,4 H-atom transfer from the methyl group to terminal O-atom via a 5-membered cyclic transition state (TS), transiently forming vinyl hydroperoxide (VHP), followed by O-O fission to yield OH + vinoxy radicals as shown in Scheme 1. Comparison of the energy-dependent unimolecular rates $k(E)$ with the computed RRKM (Rice-Ramsperger-Kassel-Marcus) rates including quantum mechanical tunneling confirmed a high-level calculation of the transition state barrier of 17.1 kcal mol^{-1} (5960 cm^{-1}) for *syn*-CH_3CHOO.[4] The unimolecular decay rates observed for *syn*-CH_3CHOO in the $2\nu_{CH}$ region (5600-6100 cm^{-1}) are on the order of 10^8 s^{-1}, corresponding to lifetimes less than 10 ns.[4] Recent work has also identified an OH roaming mechanism that results in a minor yield of thermalized hydroxycarbonyl products or hydroxymethyl [CH_2OH] and acyl [RC(O)] radicals by C-C fission of initially hot hydroxycarbonyl products.[35, 36]

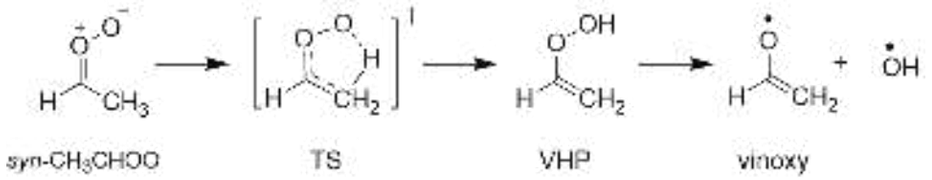

Scheme 1. 1,4 H-atom transfer mechanism for *syn* conformer of CH_3CHOO via a 5-membered cyclic transition state (TS) to vinyl hydroperoxide (VHP), followed by O-O cleavage to vinoxy and OH radical products.

The unimolecular decay dynamics of *anti*-CH_3CHOO, however, have primarily been investigated theoretically.[8, 37-39] Unimolecular decay of *anti*-CH_3CHOO is predicted to proceed via a 1,3 ring-closure mechanism in a rate limiting step that forms methyl dioxirane with a TS barrier of 15.6 kcal mol^{-1} as shown in Scheme 2.[8] Unimolecular decay is expected to continue with O-O ring opening and isomerization to form hot acetic acid [$CH_3C(O)OH$; ca. -110 kcal mol^{-1}] that can be collisionally stabilized and/or dissociate over a barrier to more stable $CH_4 + CO_2$ products [ca. -125 kcal mol^{-1}].[40-43] Theory has shown that the highly activated acid does not undergo homolysis to OH,[37] and provided an alternative explanation for an early report to the contrary.[44]

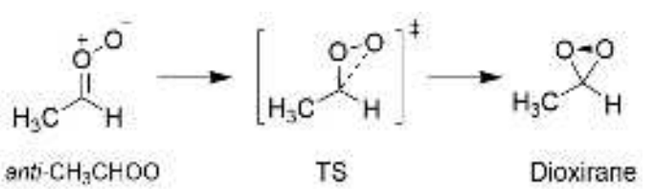

Scheme 2. 1,3-ring closure mechanism for the unimolecular decay of *anti*-CH_3CHOO via the COO ring closing TS structure to dioxirane.

Prior IR action spectroscopy studies of CH_3CHOO with OH LIF detection selectively detected the *syn* conformer, consistent with the IR spectroscopic assignments and/or unimolecular decay rates observed.[4, 14, 17] The present study utilizes an alternative IR-induced ground state depletion method for spectroscopic detection of CH_3CHOO, which should, in principle, detect both *syn* and *anti* conformers. Moreover, the unimolecular decay rate resulting from overtone CH stretch excitation ($2\nu_{CH}$) of *anti*-CH_3CHOO is expected to be even more rapid than that for *syn*-CH_3CHOO based on the lower computed TS barrier for *anti*-CH_3CHOO (ca. 15.6 kcal mol^{-1}) compared to that determined for *syn*-CH_3CHOO (17.1 kcal mol^{-1}).

It should be noted that the electronic spectrum of CH_3CHOO recorded on the strong $\pi^* \leftarrow \pi$ transition under jet-cooled conditions in this laboratory appeared to be dominated by the *syn* conformer.[10] By comparison, the analogous $B\ ^1A' \leftarrow X\ ^1A'$ absorption spectrum obtained by Sheps et al. under thermal flow cell conditions exhibited contributions from both *syn*- and *anti*-CH_3CHOO conformers, the latter extending the spectrum to longer wavelength and accounting for ca. 30% of the total population.[11] In this study, the spectra of the two structural isomers were separated by their different reactivity towards H_2O

and SO_2, which preferentially react with the *anti*-CH_3CHOO conformer. Other studies utilizing different experimental conditions and detection techniques (VUV photoionizaton,[9] IR,[15] and FTMW[19]) have reported *anti*-to-*syn* population ratios ranging from ca. 1:10 to 2:3.

The present investigation utilizes IR-VUV ion dip spectroscopy,[45-49] which is implemented by IR activation of CH_3CHOO in the overtone CH stretch ($2\nu_{CH}$) region followed by VUV photoionization detection of ground state CH_3CHOO with mass-resolved detection (m/z) using time-of-flight mass spectrometry. Prior studies have demonstrated that 10.5 eV is suitable for photoionization detection of both *syn*- and *anti*-CH_3CHOO, which have photoionization thresholds of ca. 9.4 and 9.2 eV, respectively.[9] [25] The experimental spectroscopic results are compared with new theoretical calculations that provide insights on the spectroscopic assignments of features observed in the overtone CH stretch region.

Theoretical Methods

A. Vibrational Perturbation Theory (VPT)

Calculations of the spectra were performed using second order vibrational perturbation theory (VPT2), as implemented in PyVibPT*n*.[29, 30, 50] These calculations require quartic expansions of the Hamiltonian in terms of the normal coordinates. While most implementations of vibrational perturbation theory expand the Hamiltonian in coordinates that are linear combinations of the Cartesian displacements of the atoms,[26, 51, 52] this need not be the case. When the spectrum reflects couplings among nearly degenerate vibrational levels, the expansion of the Hamiltonian in normal modes that are developed from linear combinations of displacements of internal coordinates, e.g. bond lengths and angles, can result in more accurate results.[30, 53] The coordinates used for the present study are provided in Tables ST1 and ST2. Using this choice of coordinates, the Hamiltonian that is used in the VPT2 calculations is given by

$$H = H^{(0)} + H^{(1)} + H^{(2)} \tag{1}$$

and

$$H^{(0)} = \frac{1}{2}\sum_{i,j}\left[P_i G_{ij}(\boldsymbol{r}_e)P_j + F_{ij}\Delta r_i \Delta r_j\right] \tag{2}$$

where $G_{ij}(\boldsymbol{r_e})$ represents an element of the Wilson G-matrix,[54] evaluated at the equilibrium structure, and Δr_i represents the displacement of the *i*th internal coordinate, which may be a bond length or an angle, from its value in the equilibrium geometry. Following Wilson,[54] the normal coordinates are constructed as linear combinations of the Δr_i by requiring **G** and **F** to both be diagonal. The diagonal elements of **G** and **F** in this representation are the harmonic frequencies, e.g. we construct the normal coordinates and their conjugate momenta to be dimensionless. With this transformation from the internal coordinates, the normal coordinates can be represented by **q**, and their conjugate momenta become **p**. The resulting

normal mode coordinates for *syn*-CH_3CHOO, their descriptions and harmonic frequencies are shown in Figure ST1.

Once the normal coordinates are determined, the expansion of the Hamiltonian in Eq. 1 is expressed as

$$H^0 = \sum_i \frac{\omega_i}{2}\left[p_i^2 + q_i^2\right] \tag{3}$$

$$H^{(1)} = \sum_{i,j,k}\left[\frac{1}{2}p_i\left(\frac{\partial G_{ij}}{\partial q_k}q_k\right)p_j + \frac{1}{6}\frac{\partial^3 V}{\partial q_i \partial q_j \partial q_k}q_i q_j q_k\right] \tag{4}$$

$$H^{(2)} = \frac{1}{4}\sum_{i,j,k,l} p_i\left(\frac{\partial^2 G_{ij}}{\partial q_k \partial q_l}\right)q_k q_l p_j + \sum_{i\neq j}\left[\frac{1}{8}\frac{\partial^4 V}{\partial q_i^2 \partial q_j^2}q_i^2 q_j^2 + \frac{1}{6}\frac{\partial^4 V}{\partial q_i^3 \partial q_j}q_i^3 q_j\right] + \frac{1}{2}\sum_{i\neq j\neq k}\frac{\partial^4 V}{\partial q_i^2 \partial q_j \partial q_k}q_i^2 q_j q_k + \frac{1}{24}\sum_i \frac{\partial^4 V}{\partial q_i^4}q_i^4 + V'(\boldsymbol{r}_e) \tag{5}$$

In addition to the G-matrix elements and their derivatives along with derivatives of the potential function, the final term in Eq. 5 provides a contribution to the kinetic energy operator that results from the fact that coordinates and momenta do not commute. At second order, this term provides only a constant shift to the energy and may be neglected since our interest is in transition frequencies and not the absolute energies of the states. The expression of the Hamiltonian provided by Eqs. 1 and 3 to 5 represents a restricted quartic expansion of the Hamiltonian. The terms that are not included involve fourth derivatives with respect to four different normal mode coordinates. At second order perturbation theory, these terms will contribute only if they couple nearly degenerate states. The exclusion of such terms is typically done in VPT2 calculations as these terms are expected to be small, in general. By not requiring the calculation of the mixed fourth derivatives, the evaluation of the expansion of the potential is greatly simplified as all the required terms can be obtained by numerically differentiating the Hessian with respect to each of the normal mode coordinates using a three-point finite difference scheme.

B. Handling Near Degeneracies and Adjusting Vibrational Frequencies

Because this work focuses on the spectral region that includes the overtone of the CH stretching vibrations, we expect that the states that are being accessed in the experiment will have contributions from several states that are close in energy. These would include states with different pairs of CH stretching vibrations excited and states with two or more quanta of excitation in lower-frequency vibrations. To account for this state mixing, we utilize degenerate perturbation theory. These calculations are performed in three steps. Initially we must identify which states are considered to be

nearly degenerate. This is achieved by performing a standard VPT2 calculation in which possible near-degeneracies are not considered, and identifying situations in which the perturbation theory results are likely affected by strong resonance interactions. Once this set of nearly-degenerate states has been identified, we perform a perturbation theory calculation, neglecting the contributions from $H^{(1)}$ and $H^{(2)}$ that couple the nearly-degenerate states. The resulting energies will be referred to as the deperturbed energies in the discussion that follows, and will be denoted as DVPT2 energies. Finally, we set up a small basis set calculation in the basis of the identified nearly degenerate states, where the off-diagonal elements are evaluated using second order perturbation theory. This approach has been called generalized VPT2 (GVPT2) or the deperturb and diagonalize approach.[26, 55]

While in the implementation of VPT in PyVibPT*n* the inclusion of nearly degenerate states is straightforward extension of the standard VPT2 calculation, the identification of the nearly degenerate states requires careful consideration. Several approaches have been suggested.[56, 57] The most commonly used approach is the so-called Martin test, which focuses on pairs of states and compares the energies obtained using VPT2 (without consideration of resonances) and those obtained when diagonalizing a 2×2 matrix. The diagonal elements of this matrix are the DVPT2 energies of the states of interest, while the off-diagonal elements are the matrix elements of $H^{(1)}$ evaluated in the basis of zero-order states. If the differences between the energies obtained by the two approaches exceed a threshold, then the states are considered to be degenerate.

We have explored an alternative approach, which focuses on the expansion of the state of interest in terms of eigenstates of $H^{(0)}$. If up to the desired order of perturbation theory, the contribution of a zero-order state exceeds a predetermined value, represented by χ_{max}, and the range of DVPT2 energies that is spanned by the resonance space is smaller than 500 cm^{-1}, we consider the two states to be strongly coupled. The choice of χ_{max} is important, as too large a value will miss important resonances, while a very small value will lead to solving the approximate Hamiltonian in Eq. 1 in a basis that contains all the states that are within ~ 250 cm^{-1} of the state of interest. We find that $\chi_{max} = 0.3$ provides a good compromise.[30] This value corresponds to identifying states that contribute to the eigenstate by roughly 10% or more. A comparison of the GVPT2 spectra calculated for *syn*-CH_3CHOO using several values of χ_{max} is provided in Figure ST2.

While in many cases the above approach yields spectra that are similar to those obtained using the Martin test to identify near degeneracies, we believe that using χ_{max} has several significant advantages. First, the Martin test focuses on contributions to the energy through terms in $H^{(1)}$, whereas the present approach is applied to all of the terms in the expansion of the Hamiltonian. Additionally, the Martin test focuses on the states in the initial basis, which typically consists of states with one or two quanta of excitation. In the implementation of GVPT2 in PyVibPT*n*, any state that is coupled to the state of interest

is considered. At second order, this will correspond to states with up to four quanta of excitation. Additionally, χ_{max} is dimensionless, while the Martin test compares values that have units of energy. What is considered to be a small or large deviation can vary depending on the energy of the state of interest. Finally, other properties, notably intensities, can be more sensitive to higher-order corrections to the wave function than are the energies. It is not unusual to find that a GVPT2 calculations can yield reasonable energies while the intensities are problematic. This problem is diminished when the size of the corrections to the wave function are used to identify nearly degenerate states.[30]

In the absence of near-degeneracies, VPT2 provides a good description of anharmonic systems, like *syn*-CH_3CHOO, in which the vibrational motions of interest are localized near a single minimum in the potential surface. When resonances are involved, the quality of the agreement between experiment and calculation can be very sensitive to small shifts in the depeturbed frequencies. In recent studies, we[27, 28] and others[26] have addressed this challenge by shifting the deperturbed frequencies to improve agreement with values obtained from experimental studies. This approach becomes more challenging when we are considering all of the two quanta transitions in *syn*-CH_3CHOO that involve CH stretching vibrations. *syn*-CH_3CHOO has C_s symmetry with four high-frequency normal mode vibrations ascribed to CH-stretching motions, two of which result from the motion of hydrogen atoms that lie in the COO plane (ν_1, ν_2) and two of which involve motions of the out-of-plane hydrogens, one symmetric and one asymmetric (ν_3, ν_{13}). The fundamental frequencies of the four CH stretches and ν_4 (a combination of the CO stretch and the carbonyl oxide CH wag) are known from earlier experimental studies.[15, 18] We use the difference between these frequencies and those obtained from GVPT2 calculations to shift the values of the harmonic frequencies used in subsequent GVPT2 calculations. This second set of GVPT2 calculations will be identified as *shifted* or GVPT2-sh in the following discussion. Shifting the harmonic frequencies allows us to adjust the zero-order energies of the states with two quanta of excitation in the CH stretching vibrations in an internally consistent manner. Such an approach can be viewed as being similar to the strategy utilized when optimized geometries are evaluated at a higher level of theory than vibrational frequencies, as is done in for example the Gaussian-*n* composite approaches in electronic structure theory.[58] In this case, the frequencies would be calculated at a higher level of theory than the corresponding cubic and quartic terms in the expansion of the potential. Indeed, one could use frequencies obtained at the CCSD(T) level of theory to correct the anharmonic results obtained at a lower level of theory. While in the present study we are not using multiple levels of theory for different parts of the calculation, adjusting the harmonic frequencies so that the anharmonic frequencies from GVPT2 agree with experiment is in the spirit of substituting a much higher level of electronic structure theory for the calculation of the harmonic frequencies while using the lower level of theory for the higher order derivatives.

C. Summary of Computational Approaches

For the calculations described above, we used three levels of electronic structure/basis sets B2PLYP-D3/cc-pVTZ, B3LYP/aug-cc-pVTZ, and MP2/aug-cc-pVTZ. These reflect choices that were made for previous studies of this and similar systems. All electronic structure theory calculations were performed using Gaussian 16,[59] and, unless specifically noted, the perturbation theory calculations were performed using PyVibPT*n*.[50]

Experimental Methods

The CH_3CHOO Criegee intermediate is generated from the 2,2-diiodoethane [CH_3CHI_2] precursor, as described previously.[14] In brief, CH_3CHI_2 vapor is entrained in 20% O_2/Ar carrier gas at 10 psi and pulsed through a nozzle into a quartz capillary reactor tube (1 mm I.D., ~ 25 mm length). Near the exit of the tube, 248 nm radiation from a KrF excimer laser (Coherent COMPex 102, 10 Hz, ~65 mJ/pulse, cylindrically focused) is used to photolyze the precursor, producing monoiodo CH_3CHI radicals that subsequently react with O_2 to form CH_3CHOO. The Criegee intermediates are collisionally stabilized in the capillary and cooled to a low rotational temperature upon supersonic jet expansion. The gas passes through a skimmer and is probed in a collision-free interaction region ~ 4 cm downstream, where the molecular beam is crossed with spatially-overlapped, counterpropagating IR pump and VUV probe beams.

CH_3CHOO is detected by time-of-flight mass spectrometry (TOFMS) using single photon ionization with 118 nm (10.5 eV) VUV radiation on its parent mass m/z 60. The VUV radiation is generated by frequency tripling the 355 nm output of a Nd:YAG laser (Innolas SpitLight 600, 10 Hz) in a phase-matched Xe/Ar gas mixture. CH_3CHOO is vibrationally activated using tunable IR radiation from an optical parametric oscillator/amplifier (OPO/OPA, Laservision; 0.9 cm^{-1} bandwidth) pumped by a Nd:YAG laser (Continuum Precision II 8000, 5 Hz). The IR radiation is introduced ca. 50 ns prior to VUV photoionization.

The critical spatial overlap of the focused IR radiation (~ 40 cm focal length) with the VUV radiation is optimized using a separate procedure. The optimal alignment is achieved by first ionizing the CH_3CHI_2 precursor with VUV radiation, generating $CH_3CHI_2^+$ cations, and then introducing IR radiation ca. 20 ns later that results in dissociation of the $CH_3CHI_2^+$ cations to $CH_3CHI^+ + I$. The enhancement of the CH_3CHI^+ signal (m/z 155) is then utilized to achieve the best spatial overlap of the IR and VUV beams.

In a few experiments, OH radicals resulting from unimolecular decay of IR-excited *syn*-CH_3CHOO are detected by 1+1′ resonance-enhanced multiphoton ionization (REMPI).[60, 61] For these experiments, an additional dye laser is utilized, specifically a Nd:YAG (Ekspla NL303HT, 10 Hz) pumped dye laser (NarrowScanK, Rh 590 dye, 10 Hz, ~ 1 mJ/pulse). As detailed previously,[60, 61] 1+1′ REMPI is achieved

by sequential OH A-X (1,0) excitation at ca. 281.5 nm followed by VUV excitation at 118 nm (typically delayed by 20 ns), which leads to an autoionizing *3d* Rydberg state and OH^+ cations that are detected (m/z 17). The spatial overlap of the UV and VUV beams was optimized by maximizing the UV-induced depletion of the CH_3CHOO^+ signal at m/z 60.

Experimental Results

The present study utilizes IR-VUV ion-dip spectroscopy to record the IR spectrum of CH_3CHOO in the overtone CH stretch ($2\nu_{CH}$) region under jet-cooled conditions as illustrated in Figure 2. CH_3CHOO is initially detected using time-of-flight mass spectrometry (TOFMS) with single photon VUV ionization at 118 nm (10.5 eV) on the parent mass channel m/z 60. Vibrational activation initiates unimolecular decay of *syn*-CH_3CHOO via a 1,4 H-atom transfer mechanism, releasing OH + vinoxy radical products. Similarly, vibrational activation of *anti*-CH_3CHOO results in unimolecular decay via a 1,3 ring closure mechanism to methyl dioxirane, leading to acetic acid and/or $CH_4 + CO_2$ products. [Note that acetic acid (m/z 60) will not be detected with 10.5 eV radiation due to its higher ionization energy of 10.65 eV.[62]] $2\nu_{CH}$ activation of both *syn* and *anti* conformers provides sufficient energy to surmount their respective TS barriers and lead to prompt unimolecular decay (< 10 ns, Figure SE1). As a result, IR activation of both *syn*- and *anti*-CH_3CHOO conformers is expected to result in depletion of their ground state populations and associated reduction in intensity (dip) of the VUV photoionization signal on the m/z 60 mass channel. VUV photoionization is delayed by 50 ns relative to IR excitation to provide adequate time for unimolecular decay and thereby avoid photoionization of CH_3CHOO ($2\nu_{CH}$). Alternatively, the IR action spectrum of *syn*-CH_3CHOO is obtained with photoionization detection of the OH products (m/z 17), which is analogous to prior studies utilizing OH LIF detection (Figure 2, right).[4, 14, 17]

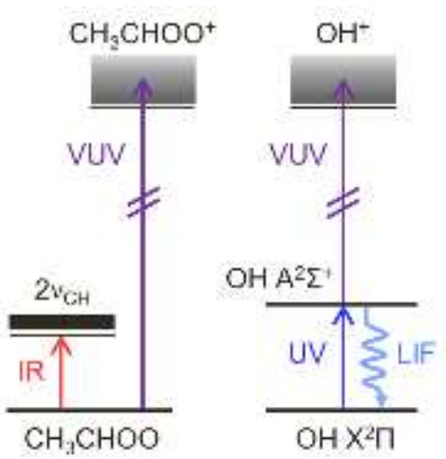

Figure 2. The IR spectra and unimolecular decay dynamics of CH_3CHOO in the overtone CH stretch ($2\nu_{CH}$) region are investigated by IR-induced ground state depletion of the VUV photoionization signal at m/z 60 (left) or IR action spectroscopy with detection of OH products by UV laser-induced fluorescence

(LIF) or 1+1′ REMPI techniques (right). The experimental detection techniques utilize 282 nm (UV) and/or 118 nm (VUV) radiation.

The IR-VUV ion dip spectrum of CH_3CHOO (m/z 60) is obtained by scanning the IR OPO over the 5650-6120 cm^{-1} range in 0.5 cm^{-1} steps. The 'IR on' signal is subtracted from a relatively constant 'IR off' ionization signal on alternating VUV laser pulses to obtain the IR spectrum shown in the top panel of Figure 3. A significant IR induced depletion of the VUV photoionization signal is observed upon IR activation at 5984 and 6081 cm^{-1} (Figure SE2), while weaker features are observed in the 5700 to 5900 cm^{-1} region. The percentage depletion, $[(IR_{off} - IR_{on})/IR_{off})] \times 100\%$, of the two prominent peaks at 5984 and 6081 cm^{-1} are ~30% and ~22%, respectively, based on Gaussian fits of their mass peaks.

The ion dip spectrum for CH_3CHOO is compared with previously reported IR action spectrum for *syn*-CH_3CHOO obtained via the OH LIF detection method in Figure 3. Both experimental spectra exhibit a similar pattern of IR transitions, particularly in the spectral regions around 5700, 5984 and 6081 cm^{-1}. The similarity observed between the IR ion dip spectrum and the IR action spectrum indicates that the primary spectral carrier in the ion-dip spectrum is the *syn* conformer.

The *anti* conformer is predicted to have a distinctly different IR spectrum in the overtone CH stretch ($2\nu_{CH}$) region (see Figures SE4 and ST3), as might be expected since it lacks the intramolecular hydrogen bonding interaction between the methyl group and terminal O atom of the *syn* conformer. However, the strongest predicted *anti* transition at ca. 5770 cm^{-1} (Table ST3) with comparable predicted intensity as predicted for the *syn* conformer (Tables ST4) is not observed. (Other weaker *anti* transitions predicted in the 5900-6000 cm^{-1} region would not be distinct because they overlap strong *syn* transitions.) This is consistent with a low abundance of the *anti* conformer. Prior experimental studies utilizing a wide range of spectroscopic techniques have shown that *syn*-CH_3CHOO is preferentially generated compared to *anti*-CH_3CHOO (*anti* accounts for < 40% of the two conformers)[9-11, 15, 19] using the alternate synthetic approach for producing the Criegee intermediates.

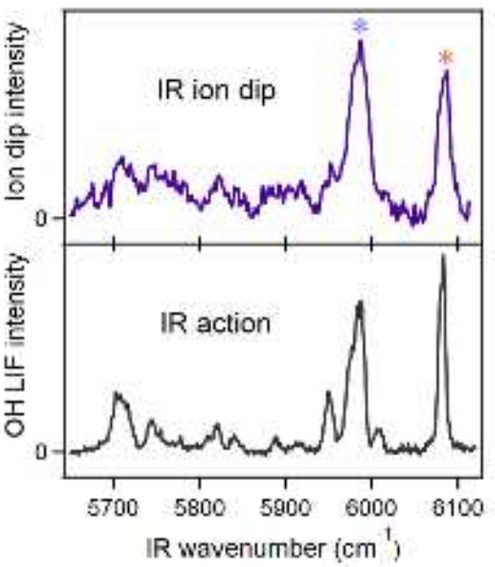

Figure 3. Experimental IR ion-dip spectrum (top) and previously reported IR action spectrum (bottom) of CH_3CHOO in the overtone CH stretch ($2\nu_{CH}$) region from 5650 to 6120 cm^{-1}. The two prominent peaks in the ion-dip spectrum at 5984 cm^{-1} and 6081 cm^{-1} are indicated by blue and red asterisks, respectively. The bottom trace is adapted from Ref. 14.

Despite the clear similarity of the IR ion dip and IR action spectra, there are notable differences, in particular the breadth and relative intensity of the dominant features at 5984 and 6081 cm^{-1}. These changes can be understood by closer examination of the rotational band contour for the 6081 cm^{-1} feature, which is slightly broader with a weaker relative peak intensity in the IR ion dip spectrum compared to the IR action spectrum. The rotational band contours were simulated in Figure 4 using the experimental laser linewidth and typical homogeneous broadening due to intramolecular vibrational energy redistribution (1.7 cm^{-1} Lorentzian), along with rotational constants from a prior FTWM study[19] and computed near equal a:b transition type contributions (see SI Sec. SE4 for additional details). However, the IR ion dip feature exhibits a rotational band contour characteristic of a ca. 43 K rotational temperature compared to the ca. 10 K rotational temperature obtained in the IR action spectrum. This can be understood by the different backing gas pressures used in the two experiments with 10 psi of 20% O_2/Ar carrier gas used in the ion dip study and 30 psi of the same gas mixture used in the prior LIF study. Nevertheless, the rotational band contours have the same integrated intensities (Figure 4, solid lines). Therefore, the different breadths and relative intensities of the experimental 6081 cm^{-1} features can be mainly attributed to the different rotational temperatures achieved in two experimental setups. In contrast, the 5984 cm^{-1} feature is less sensitive to rotational temperature change, as shown in Figure SE5. This feature likely involves multiple underlying transitions and/or more complicated coupling between various modes, as evident from its broader spectral profile.

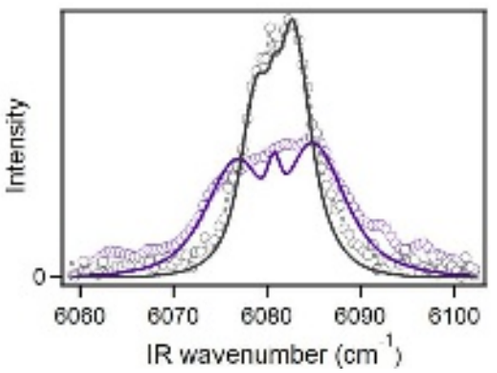

Figure 4. Rotational band contour fits (solid lines) and the experimental data (points) of the 6081 cm^{-1} feature recorded with the IR ion-dip (purple) and IR action (black, Ref. 14) spectroscopy methods. The simulated traces show that the change in the band contour arises from the different rotational temperatures achieved in the two experiments, specifically 43 K (ion dip) compared to 10 K (action), but notably the band origin, spectral linewidth, and integrated areas of the band contours are unchanged.

Finally, IR excitation *syn*-CH_3CHOO in the $2\nu_{CH}$ region yields OH products, which have been detected in this study by 1+1′ REMPI utilizing OH A-X (1,0) $R_1(1.5)$ excitation at 281.5 nm and VUV ionization at 118 nm (Figure 2, right).[60, 61] The OH REMPI signals detected at m/z 17 resulting from IR activation of *syn*-CH_3CHOO at 5984 and 6081 cm^{-1} are shown in Figure SE3. In each case, OH background (IR off) arising from prompt unimolecular decay of energized CH_3CHOO within the capillary tube has been subtracted.

The IR-induced changes in the photoion signals for CH_3CHOO (m/z 60) and OH radical (m/z 17) are measured concurrently for comparison in Figure 5. The integrated CH_3CHOO photoion signal (m/z 60) obtained upon IR activation at 6081 cm^{-1} compared to that at 5984 cm^{-1} yields a ratio of ca. 83%. Similarly, integration of the OH ion signal (m/z 17) measured upon IR excitation at 6081 cm^{-1} compared to 5984 cm^{-1} exhibits a ratio of ca. 85%. These two ratios are equivalent considering the 2-3% uncertainty in the depletion measurements.[60, 61, 63] The similar OH radical yields upon IR activation of CH_3CHOO at 5984 and 6081 cm^{-1} provides further evidence for the dominant contribution of the *syn*-CH_3CHOO conformer to the IR spectrum at these energies.

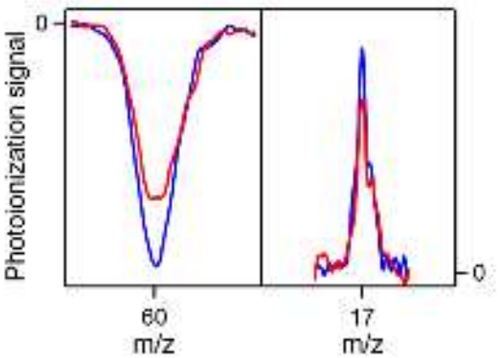

Figure 5. IR-induced depletion of the CH_3CHOO photoionization signal (m/z 60, left) and the corresponding IR-induced OH product photoionization signal (m/z 17, right) upon IR excitation of $2\nu_{CH}$ transitions at 5984 cm^{-1} (blue) and 6081 cm^{-1} (red).

Theoretical Results

The GVPT2 results obtained in the $2\nu_{CH}$ region using the B2PLYP-D3/cc-pVTZ electronic structure method/basis set (dark green, bottom panel) are compared to the experimental spectrum (top panel) in Figure 6. The agreement between the measured and calculated spectra is good in the lower energy region near 5700 cm^{-1}. Near 6000 cm^{-1}, there is only a single peak in the GVPT2 spectrum (labeled I), while there are two peaks with significant intensity (7 and 9) in the measured spectrum. This deviation between calculation and experiment makes it difficult to assign the spectrum in this region.

The discrepancies between experiment and calculation in this spectral region can be traced to the fact that there are many nearly degenerate states in this energy range. The GVPT2 calculation used to obtain the spectrum in the bottom panel of Figure 6 required a resonance space that contains 44 states. As a result, many of the accessed states are mixed in character (see Tables 1 and ST4, which provide the decomposition of the states based on the contributions from the states obtained from the DVPT2 calculation). A consequence of this mixed character is that small changes in the deperturbed (DVPT2) energies of these states can have a notable effect on the mixing, and from that the frequencies and intensities of the transitions in the calculated spectrum. This leaves a large parameter space that could be explored if we want to make small adjustments to the calculated state energies to bring the calculation into better agreement with experiment. As we consider possible adjustments, they should be physically motivated. As noted above, in adjusting the calculated spectrum we draw on information from studies of lower-energy transitions to introduce shifts in the deperturbed frequencies of the transitions in this higher energy region of the spectrum.

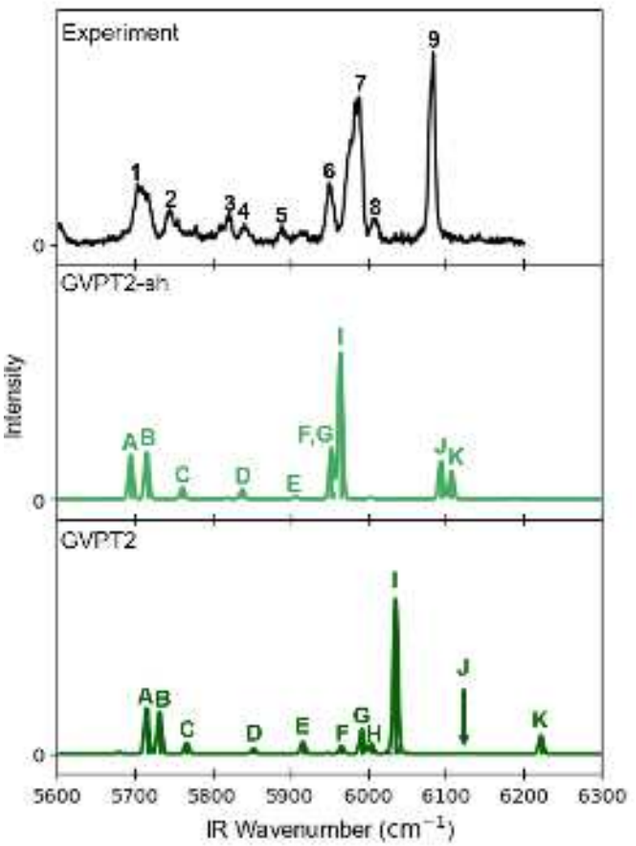

Figure 6. (Top) Infrared transitions experimentally observed for *syn*-CH_3CHOO in the overtone CH stretch ($2\nu_{CH}$) region and adapted from Ref. 14. Comparison with theoretically predicted spectra obtained from a GVPT2 calculation (bottom, dark green) and a GVPT2-sh calculation (middle, light green) in which some of the harmonic frequencies have been shifted by the amounts indicated in Table 2. The VPT2 calculations are based on electronic structure calculations performed using the B2PLYP-D3/cc-pVTZ electronic structure method/basis. The frequencies, intensities and assignments of the transitions in the calculated spectra are provided in Tables 1 and ST4.

Table 1. Infrared transitions (cm^{-1}) computed and observed in the overtone CH stretch ($2\nu_{CH}$) spectral region for *syn*-CH_3CHOO with GVPT2 based on electronic structure calculations performed using the B2PLYP-D3/cc-pVTZ electronic structure method/basis.

	Calculation			Experiment	
Label	Assignment[a] (shifted)	GVPT2-sh[b]	GVPT2[b,c]	Frequency[d]	Label
A	$2\nu_3$ (59%), $2\nu_{13}$(26%), $\nu_3 + 2\nu_5$(11%)	5694.9	5715.2	5709.0	1
B	$\nu_3 + \nu_{13}$	5715.4	5731.9		
C	$\nu_3 + 2\nu_5$ (80%), $2\nu_{13}$(14%)	5761.4	5766.7	5747.6	2
D	$2\nu_{13}$ (53%), $2\nu_3$(37%)	5838.3	5852.8	5818.1	3
E	$\nu_2 + \nu_3$	5906.2	5915.8		
F	$\nu_2 + \nu_{13}$	5953.7	5965.7	5950.9	6
G	$2\nu_2$	5952.7	5991.6		
H	$\nu_1 + \nu_3$	5978.3	6004.4		
I	$2\nu_1$(66%), $\nu_1 + 2\nu_4$ (30%)	5964.3	6035.3	5983.5	7
J	$\nu_1 + \nu_2$ (73%), $\nu_1 + 2\nu_4$ (21%)	6093.4	6134.7	6080.7	9
K	$\nu_1 + 2\nu_4$ (47%), $2\nu_1$(32%), $\nu_1 + \nu_2$(19%)	6107.2	6222.1		

a. Assignments are based on the results of the GVPT2-sh calculations. Percentages reflect the percent contributions based on the diagonalization of the Hamiltonian in the space of nearly degenerate spaces. Contributions of greater than 10% are included and the sum of the contributions add up to at least 80% of the total amplitude.
b. GVPT2 and shifted GVPT2 (GVPT2-sh) calculations are performed using PyVibPT*n*.
c. Assignments for the GVPT2 transitions are provided in Table ST4.
d. Ref. 14.

As background, we start by reviewing a prior IR spectroscopic study of jet-cooled *syn*-CH_3CHOO in the fundamental CH stretch region, shown in Figure 7 (top panel), which included rotational band contour analyses of the observed features.[18] The features centered at 2907.8 and 3020.0 cm^{-1} (labeled I and IV) had *a*/*b*-type parallel transitions, which were ascribed as ν_3 methyl out-of-plane symmetric CH stretch and ν_2 methyl in-plane CH stretch. A feature centered at 2935 cm^{-1} (labeled II/III) was composed of two overlapping transitions: a *c*-type perpendicular transition with origin at 2932.0 cm^{-1} assigned as the ν_{13} methyl out-of-plane asymmetric stretch (labeled III in Table 2) and an *a*/*b*-type band at 2934.8 cm^{-1} assigned to the overtone in ν_4 (labeled II in Table 2) which has both CO stretching and carbonyl oxide CH wagging character. An additional feature at 3078 cm^{-1} was attributed to the carbonyl oxide CH stretch ν_1 (labeled V). The theoretical analysis that follows shows that features I and II have highly mixed vibrational character that was not evident in the earlier study.

Next, in Figure 7 we compare the experimental and calculated spectra in the fundamental CH stretch region from 2900 to 3100 cm^{-1}. The energies of the calculated transitions are summarized in Table 2 and

compared with the prior experimental observations.[18] While the agreement between the calculated GVPT2 spectrum (Figure 7, bottom panel) and the experimental spectrum is better than in the higher energy region, the calculated transition energies deviate by up to 20 cm^{-1} from the measured values. Additionally, the three peaks near 2900 cm^{-1} overlap in the calculated spectrum. Following the procedure described above, the harmonic frequencies for the four CH stretches (modes 1 to 3 and 13) and mode 4 (see Figure ST1 for illustrations of the normal modes in *syn*-CH_3CHOO) were shifted by the difference between the measured peak position and the calculated fundamental frequency. This resulted in empirical shifts of 0 to +20 cm^{-1} (in 5 cm^{-1} increments), as reported in Table 2. The adjusted harmonic frequencies are then used in the perturbation theory. These shifts will affect the zero-order energies, which in turn will affect the higher-order corrections to the energies as these are inversely proportional to differences between zero-order energies. The resulting spectrum is plotted in light green in the middle panel of Figure 7, and the corresponding energies are reported in the GVPT2-sh column of Table 2. This procedure brought the computed frequencies and intensities, particularly for features e and f in Figure 7, into near quantitative agreement with the experimental observations, most notably for features IV and V. The results of the GVPT2-sh calculation confirm that features d, e, and f can be assigned as nearly pure fundamental ν_{13}, ν_2, and ν_1 transitions, respectively. By contrast, the GVPT2-sh results revealed that features a and b are heavily mixed transitions involving predominantly ν_3 and $2\nu_4$, respectively. The frequencies of experimental features I, II, and III are in close accord with computed features a, b, and d, suggesting analogous mixed composition for two (a, b) of these observed features.

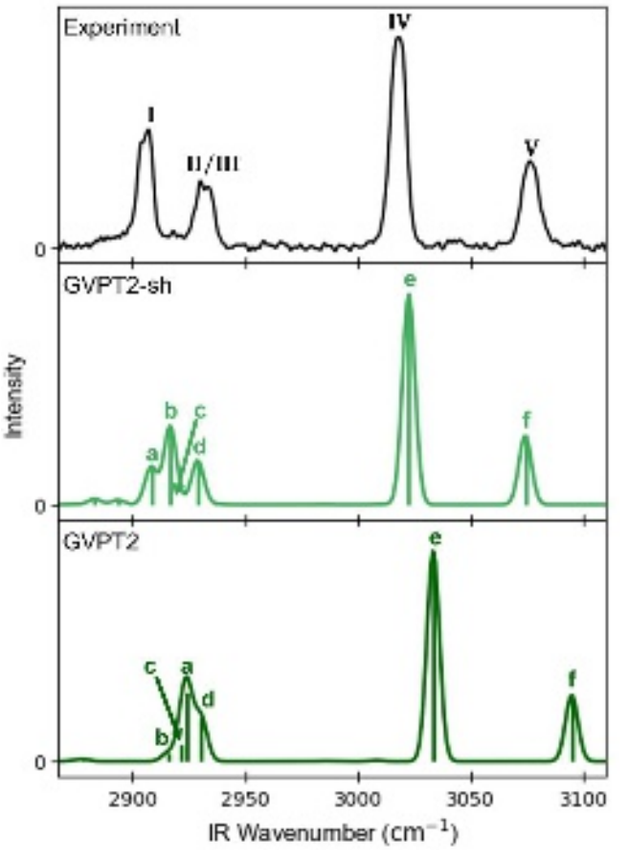

Figure 7. (Top) Infrared transitions experimentally observed for *syn*-CH_3CHOO in the fundamental CH stretch region and adapted from Ref. 18. Comparison with theoretically predicted spectra obtained from a GVPT2 calculation (bottom, dark green) and a GVPT2-sh calculation (middle, light green) in which some harmonic frequencies have been shifted by the amounts indicated in Table 2 based on electronic structure calculations performed using the B2PLYP-D3/cc-pVTZ electronic structure method/basis. The frequencies, intensities and assignments of the transitions in the calculated spectra are provided in Tables 2 and ST5.

Table 2. Infrared transitions (cm^{-1}) computed and observed in the fundamental CH stretch spectral region for *syn*-CH_3CHOO with VPT2 using the B2PLYP-D3/cc-pVTZ electronic structure method/basis.

	Calculation				Experiment	
Label	Assignment[a]	GVPT2-sh[b]	GVPT2[b,c]	shift[d]	Frequency[e]	Label
	ν_4	1474.6	1475.2	+0	1476.8	
a	ν_3 (47%), $2\nu_4$ (28%), $2\nu_5$ (10%)	2908.2	2924.0	+15	2907.8	I
b	$2\nu_4$ (58%), ν_3 (23%)	2916.7	2915.7	2(+0)	2934.8	II
c	$\nu_5 + \nu_8 + 2\nu_{18}$ (65%), $\nu_8 + \nu_{15} + 2\nu_{18}$ (22%)	2919.6	2921.9			
d	ν_{13}	2928.8	2930.4	+0	2932.0	III
e	ν_2	3022.5	3033.3	+10	3020.0	IV
f	ν_1	3074.2	3094.8	+20	3078.0	V

a. Assignments are based on the results of the GVPT2-sh calculations. Percentages reflect the percent contributions based on the diagonalization of the Hamiltonian in the space of nearly degenerate spaces. Contributions of greater than 10% are included and the sum of the contributions add up to at least 80% of the total amplitude.
b. GVPT2 and shifted GVPT2 (GVPT2-sh) calculations are performed using PyVibPT*n*.
c. Assignments for the GVPT2 transitions are provided in Table ST5.
d. Shift of the harmonic frequencies used in the GVPT2-sh calculations.
e. Refs. 15, 18.

Having demonstrated the efficacy of the approach in the fundamental CH stretch (ν_{CH}) region, we return to the higher energy overtone CH stretch ($2\nu_{CH}$) region. Using the same shifts of harmonic frequencies, we obtain the spectrum plotted in the middle panel of Figure 6. The corresponding energies are reported in Table 1, along with the assignments that are obtained from analysis of the GVPT2 wave functions, where the states are obtained from the DVPT2 calculation, described above. As can be seen, some of the transitions (e.g. those labeled B, E and F) reflect transitions to states that are well-described by a single zero-order deperturbed state, while other states are highly mixed. It is this mixing that, for example, leads to the additional peak (identified as J and K) near 6100 cm^{-1}.

Overall, the agreement between the experimental spectrum in the $2\nu_{CH}$ region and the calculated spectrum obtained using the shifted harmonic frequencies (GVPT2-sh) is much better than that resulting from the original GVPT2 calculation. There are two important differences between the two sets of GVPT2 calculations. First, we have altered the zero-order energy of the states that are accessed in these transitions. This leads to shifts in the deperturbed energies that make up the diagonal elements of the Hamiltonian matrix involving the nearly degenerate states. The second factor comes from changes in the mixings of the zero-order states with these shifts. In other words, changing the deperturbed energies of the states included in the diagonalization step of the GVPT2 calculation will affect energies and wave

functions that are obtained when the Hamiltonian matrix is diagonalized. Even small energy changes can have noticeable consequences in the resulting spectrum.

To explore the contributions of these two factors, in Figures ST4 and ST5 we compare the DVPT2 and DVPT2-sh spectra (e.g. the spectra obtained by considering energies and wave functions obtained from a DVPT2 calculation prior to matrix diagonalization). Comparing these two traces in the overtone region, which are shown in red in the bottom two panels of Figure ST4, we find that the differences between them can be accounted for by the shifts in the harmonic frequencies. The intensities of the DVPT2 spectra are not affected by this shift. Additionally, the DVPT2 spectrum closely resembles the spectrum obtained from a GVPT2 calculation performed using Gaussian 16, which is consistent with the smaller resonance space used in GVPT2 calculations preformed using G16 compared with those obtained using PyVPT*n*. The changes in the intensities between the two spectra plotted in Figure 6 reflect changing in the mixing of these deperturbed states. This points to the challenges in assigning the spectra to specific transitions as small shifts in the energies of the deperturbed states can have a significant effect on the spectral envelope.

While the above results are encouraging, they raise the questions of how robust the approach is, and whether one could base the shifts on harmonic frequencies calculated at a higher level of electronic structure theory. In particular, how sensitive are the results to the level of electronic structure theory that is used for the calculations. We repeated the calculation of the spectrum of *syn*-CH_3CHOO in both regions using the MP2/aug-cc-pVTZ and B3LYP/aug-cc-pVTZ levels of theory and basis sets. The results of GVPT2 calculations with and without shifts to the harmonic frequencies are provided in Figures ST6 and ST7 and the corresponding shifts are provided in Tables ST6 to ST8. While there are notable differences among the spectra obtained at these levels of theory when we use the harmonic frequencies that come from the calculations, once the harmonic frequencies for modes 1 to 4 and 13 have been shifted so the GVPT2 energies match the previously measured values, the three spectra become nearly indistinguishable. We have also calculated the spectra of *syn*-CH_3CHOO at the B2PLYP-D3/cc-pVTZ level of theory, shifting the harmonic frequencies to match those obtained at the CCSD(T)/ANO0 level of theory/basis.[64] The results of this calculation, which are provided in Figures ST12 and ST13 agree well with the measured spectrum. These results provide further validation of the approach.

We have repeated this analysis for a combination band spectral region (CH stretch combined with a lower frequency mode) of *syn*-CH_3CHOO that has been previously reported,[16] and the results of this analysis are provided in Figure ST8 and Table ST9. The agreement between experiment and calculation is comparable to that reported in the original study and no changes in assignments were suggested by this work.

In contrast, selective deuteration of the methyl group of the Criegee intermediate simplified its infrared action spectrum in the overtone CH stretch region, as the three CD stretches shift to ca. 2200 cm^{-1} compared to the CH stretch at ca. 3000 cm^{-1}. Specifically, the $2\nu_1$ transition associated with the single CH oscillator became an isolated feature at 6055.0 cm^{-1}, which was observed via LIF detection of OD products (Figure ST9).[17] The calculated (GVPT2) spectrum shows a pair of peaks with nearly equal intensity at 5988 and 6121 cm^{-1}, J and K in Figure ST9). These are assigned as $2\nu_1$ and $\nu_1 + 2\nu_4$, which are coupled through a 2:1 Fermi resonance. This strong coupling can be attributed to the significant carbonyl oxide CH wagging character in mode 4. The corresponding deperturbed energy of the $2\nu_1$ transition is 6052 cm^{-1} (Table ST13) which is in good agreement with the spectrum, and a slight shift in the energy of either of these states will have a significant impact on the extent of the mixing. It will also impact the relative intensities of the two transitions. Comparison with the CH overtone region of CH_3CHOO (Figure 6 and Table 1) shows the extent of shifting and mixing of the ν_1 character across several spectral features (I and K), and contributing to the intensity of experimental features spanning 100 cm^{-1} (7 and 9). The shift in the position of the transition associated with the overtone in this CH stretching vibration in CD_3CHOO compared to CH_3CHOO reflects that the corresponding normal mode in *syn*-CH_3CHOO has contributions from several CH stretching vibrations, as is seen in Figure ST1. In contrast, the normal mode in CD_3CHOO corresponds to the motion of the lone CH oscillator. Comparisons of the calculated spectra for various partially deuterated forms of the *syn*-methyl-substituted Criegee intermediate are shown in Figure ST11, with assignments provided in Table ST12. While there are shifts in the positions of the peaks, as with CD_3CHOO, they can be accounted for by the mixed nature of the normal modes. Finally, for completeness, the calculated spectrum for CD_3CDOO and its assignment are provided in Figure ST10 and Table ST11.

Conclusions

IR-VUV ion-dip spectroscopy is implemented to examine the IR spectrum of the methyl-substituted Criegee intermediate (CH_3CHOO) in the overtone CH stretch ($2\nu_{CH}$) region utilizing VUV photoionization detection of ground state CH_3CHOO. Although both *syn* and *anti* conformers of CH_3CHOO may be detected with this approach, the observed spectrum – including the major features at 5984 and 6081 cm^{-1} – is attributed to the more stable *syn*-CH_3CHOO conformer. The predominance of the *syn* conformer stems from its significantly greater population when prepared using an alternate laboratory synthesis combined with supersonic jet-cooling. The assignment of the IR-VUV ion-dip spectrum to the *syn* conformer is confirmed by comparison with a prior IR action spectrum obtained with OH product laser-induced fluorescence detection[14] and an analogous IR-induced UV+VUV photoionization signal of the OH product in this study. The OH product originates from rapid

unimolecular decay of the *syn* conformer via 1,4 H-atom transfer and O-O bond cleavage.[4] The IR spectrum of *syn*-CH_3CHOO in the overtone CH stretch region is quite complicated and not readily assigned, although prior attempts have been made based on second order vibrational perturbation theory as implemented in Gaussian 16.[14] The difficulty arises from the many combinations of two quanta of excitation involving the four CH stretch vibrations (ν_1, ν_2, ν_3, and ν_{13}) along with couplings among these and other nearby vibrational states.

By utilizing a general implementation of vibrational perturbation theory (VPT), we gain insights into the vibrations responsible for the features in the experimental spectrum. We find that by shifting the harmonic frequencies by up to 20 cm^{-1} based on differences between experimental and calculated transitions in the fundamental CH stretch region, we can achieve excellent agreement between experiment and theory in the overtone CH stretch region. The most intense features observed in the overtone CH stretch region at 5984 and 6081 cm^{-1} (features 7 and 9) are ascribed to highly mixed states having contributions from two quanta of CH stretch ($2\nu_1$ or $\nu_1 + \nu_2$) and/or a combination of CH stretch with two quanta in mode 4 ($\nu_1 + 2\nu_4$). This empirical approach was implemented using three different levels of electronic structure theory/basis sets: B2PLYP-D3/cc-pVTZ, B3LYP/aug-cc-pVTZ, and MP2/aug-cc-pVTZ, and using harmonic frequencies calculated at the CCSD(T)/ANO0 level to determine the shifts for the GVPT2 calculation. For all levels of electronic structure theory, the resulting spectra are virtually indistinguishable from each other, illustrating the robustness of this approach.

Supporting Information Description

The Supporting Information contains statistical unimolecular decay rates for *anti*-CH_3CHOO; mass spectra of the CH_3CHOO and OH products; fits to rotational band contours; calculated spectra for *anti*-CH_3CHOO as well as *syn*-CH_3CHOO in other spectral regions; the effects of deuteration on the spectrum of *syn*-CH_3CHOO; descriptions of the coordinates used in this study; additional discussion of the VPT2 calculations; values of the calculated frequencies and intensities used to generate the calculated spectra; an EXCEL file containing the Hamiltonian matrices generated in the GVPT2 calculations.

Acknowledgments

Experimental research at the University of Pennsylvania supported by the National Science Foundation under grants CHE-1955068 and CHE-2301298. Partial equipment support was provided by the US Department of Energy, Office of Science, Basic Energy Sciences under grant DE-FG02-87ER13792. T.K.R. was primarily supported by a Walter-Benjamin Scholarship funded by the Deutsche Forschungsgemeinschaft (DFG, German Research Foundation) - Project number 508074809. Theoretical research at the University of Washington supported by the National Science Foundation under grant CHE-2154126. The authors thank Stephen J. Klippenstein (Argonne) and Mark A. Boyer (Univ. Wisconsin) for helpful discussions. We specifically thank S.J.K. and reviewer 1 for suggesting that we shift the spectra based on harmonic frequencies evaluated at the CCSD(T) level of theory.

References

[1] R. Criegee, "Mechanism of Ozonolysis," Angew. Chem. Int. Edit. **14**, 745-752 (1975).
[2] K. Sindelarova, C. Granier, I. Bouarar, A. Guenther, S. Tilmes, T. Stavrakou, J. F. Müller, U. Kuhn, P. Stefani and W. Knorr, "Global data set of biogenic VOC emissions calculated by the MEGAN model over the last 30 years," Atmos. Chem. Phys. **14**, 9317-9341 (2014).
[3] N. M. Donahue, G. T. Drozd, S. A. Epstein, A. A. Presto and J. H. Kroll, "Adventures in ozoneland: down the rabbit-hole," Phys. Chem. Chem. Phys. **13**, 10848-10857 (2011).
[4] Y. Fang, F. Liu, V. P. Barber, S. J. Klippenstein, A. B. McCoy and M. I. Lester, "Communication: Real Time Observation of Unimolecular Decay of Criegee Intermediates to OH Radical Products," J. Chem. Phys. **144**, 061102 (2016).
[5] D. Johnson and G. Marston, "The gas-phase ozonolysis of unsaturated volatile organic compounds in the troposphere," Chem. Soc. Rev. **37**, 699-716 (2008).
[6] D. L. Osborn and C. A. Taatjes, "The physical chemistry of Criegee intermediates in the gas phase," Int. Rev. Phys. Chem. **34**, 309-360 (2015).
[7] K. J. Heaton, R. L. Sleighter, P. G. Hatcher, W. A. Hall and M. V. Johnston, "Composition Domains in Monoterpene Secondary Organic Aerosol," Environ. Sci. Technol. **43**, 7797-7802 (2009).
[8] B. Long, J. L. Bao and D. G. Truhlar, "Atmospheric Chemistry of Criegee Intermediates: Unimolecular Reactions and Reactions with Water," J. Am. Chem. Soc. **138**, 14409-14422 (2016).
[9] C. A. Taatjes, O. Welz, A. J. Eskola, J. D. Savee, A. M. Scheer, D. E. Shallcross, B. Rotavera, E. P. Lee, J. M. Dyke, D. K. Mok, D. L. Osborn and C. J. Percival, "Direct Measurements of Conformer-Dependent Reactivity of the Criegee Intermediate CH_3CHOO," Science **340**, 177-180 (2013).
[10] J. M. Beames, F. Liu, L. Lu and M. I. Lester, "UV Spectroscopic Characterization of an Alkyl Substituted Criegee Intermediate CH_3CHOO," J. Chem. Phys. **138**, 244307 (2013).
[11] L. Sheps, A. M. Scully and K. Au, "UV Absorption Probing of the Conformer-Dependent Reactivity of a Criegee Intermediate CH_3CHOO," Phys. Chem. Chem. Phys. **16**, 26701-26706 (2014).
[12] Y. L. Li, M. T. Kuo and J. M. Lin, "Unimolecular Decomposition Rates of a Methyl-Substituted Criegee Intermediate *syn*-CH_3CHOO," Rsc Adv. **10**, 8518-8524 (2020).
[13] C. Robinson, L. Onel, J. Newman, R. Lade, K. D. Au, L. Sheps, D. E. Heard, P. W. Seakins, M. A. Blitz and D. Stone, "Unimolecular Kinetics of Stabilized CH_3CHOO Criegee Intermediates: *syn*-CH_3CHOO Decomposition and *anti*-CH_3CHOO Isomerization," J. Phys. Chem. A **126**, 6984-6994 (2022).
[14] F. Liu, J. M. Beames, A. S. Petit, A. B. McCoy and M. I. Lester, "Infrared-Driven Unimolecular Reaction of CH_3CHOO Criegee Intermediates to OH Radical Products," Science **345**, 1596-1598 (2014).
[15] H.-Y. Lin, Y.-H. Huang, X. Wang, J. M. Bowman, Y. Nishimura, H. A. Witek and Y.-P. Lee, "Infrared Identification of the Criegee Intermediates *syn*- and *anti*-CH_3CHOO, and Their Distinct Conformation-Dependent Reactivity," Nat. Commun. **6**, 7012 (2015).
[16] Y. Fang, F. Liu, V. P. Barber, S. J. Klippenstein, A. B. McCoy and M. I. Lester, "Deep Tunneling in the Unimolecular Decay of CH_3CHOO Criegee Intermediates to OH Radical Products," J. Chem. Phys. **145**, 234308 (2016).
[17] A. M. Green, V. P. Barber, Y. Fang, S. J. Klippenstein and M. I. Lester, "Selective Deuteration Illuminates the Importance of Tunneling in the Unimolecular Decay of Criegee Intermediates to Hydroxyl Radical Products," Proc. Natl. Acad. Sci. U.S.A. **114**, 12372-12377 (2017).
[18] V. P. Barber, S. Pandit, V. J. Esposito, A. B. McCoy and M. I. Lester, "CH Stretch Activation of CH_3CHOO: Deep Tunneling to Hydroxyl Radical Products," J. Phys. Chem. A **123**, 2559-2569 (2019).
[19] M. Nakajima and Y. Endo, "Communication: Spectroscopic Characterization of an Alkyl Substituted Criegee Intermediate *syn*-CH_3CHOO through Pure Rotational Transitions," J. Chem. Phys. **140**, 011101 (2014).
[20] M. Nakajima, Q. Yue and Y. Endo, "Fourier-Transform Microwave Spectroscopy of an Alkyl Substituted Criegee Intermediate *anti*-CH_3CHOO," J. Mol. Spectrosc. **310**, 109-112 (2015).

[21] T. Berndt, T. Jokinen, M. Sipila, R. L. Mauldin, H. Herrmann, F. Stratmann, H. Junninen and M. Kulmala, "H_2SO_4 Formation from the Gas-Phase Reaction of Stabilized Criegee Intermediates with SO_2: Influence of Water Vapour Content and Temperature," Atmos. Environ. **89**, 603-612 (2014).
[22] L. C. Lin, H. T. Chang, C. H. Chang, W. Chao, M. C. Smith, C. H. Chang, J. J. M. Lin and K. Takahashi, "Competition Between H_2O and $(H_2O)_2$ Reactions with CH_2OO/CH_3CHOO," Phys. Chem. Chem. Phys. **18**, 4557-4568 (2016).
[23] N. U. M. Howes, Z. S. Mir, M. A. Blitz, S. Hardman, T. R. Lewis, D. Stone and P. W. Seakins, "Kinetic Studies of C_1 and C_2 Criegee Intermediates with SO_2 Using Laser Flash Photolysis Coupled with Photoionization Mass Spectrometry and Time Resolved UV Absorption Spectroscopy," Phys. Chem. Chem. Phys. **20**, 22218-22227 (2018).
[24] W. Chao, Y. H. Lin, C. T. Yin, W. H. Lin, K. Takahashi and J. J. M. Lin, "Temperature and Isotope Effects in the Reaction of CH_3CHOO with Methanol," Phys. Chem. Chem. Phys. **21**, 13633-13640 (2019).
[25] M. F. Vansco, M. Zou, I. O. Antonov, K. Ramasesha, B. Rotavera, D. L. Osborn, Y. Georgievskii, C. J. Percival, S. J. Klippenstein, C. A. Taatjes, M. I. Lester and R. L. Caravan, "Dramatic Conformer-Dependent Reactivity of the Acetaldehyde Oxide Criegee Intermediate with Dimethylamine Via a 1,2-Insertion Mechanism," J. Phys. Chem. A **126**, 710-719 (2022).
[26] P. R. Franke, J. F. Stanton and G. E. Douberly, "How to VPT2: Accurate and Intuitive Simulations of CH Stretching Infrared Spectra Using VPT2+K with Large Effective Hamiltonian Resonance Treatments," J. Phys. Chem. A **125**, 1301-1324 (2021).
[27] S. J. Stropoli, T. Khuu, M. A. Boyer, N. V. Karimova, C. F. Gavin-Hanner, S. Mitra, A. L. Lachowicz, N. Yang, R. B. Gerber, A. B. McCoy and M. A. Johnson, "Electronic and Mechanical Anharmonicities in the Vibrational Spectra of the H-bonded, Cryogenically Cooled $X^- \cdot HOCl$ (X=Cl, Br, I) Complexes: Characterization of the Strong Anionic H-bond to an Acidic OH Group," J. Chem. Phys. **156**, 174303 (2022).
[28] J. A. Lau, M. DeWitt, M. A. Boyer, M. C. Babin, T. Solomis, M. Grellmann, K. R. Asmis, A. B. McCoy and D. M. Neumark, "High-Resolution Photoelectron Spectroscopy of Vibrationally Excited Vinoxide Anions," J. Phys. Chem. A **127**, 3133-3147 (2023).
[29] M. A. Boyer and A. B. McCoy, "A Flexible Approach to Vibrational Perturbation Theory Using Sparse Matrix Methods," J. Chem. Phys. **156**, 054107 (2022).
[30] M. A. Boyer and A. B. McCoy, "A Wave Function Correction-Based Approach to the Identification of Resonances for Vibrational Perturbation Theory," J. Chem. Phys. **157**, 164113 (2022).
[31] J. J. Sakurai, *Modern Quantum Mechanics*, Revised ed.,(Addison-Wesley Pub. Co., Reading, Mass. :, 1994).
[32] T. Kato, *Perturbation Theory for Linear Operators*, Second ed.,(Springer-Verlag, New York :, 1976).
[33] A. B. McCoy and M. A. Duncan, "Evidence of anharmonicity in the vibrational spectrum of protonated ethylene," J. Mol. Spectrosc. **389**, 111704 (2022).
[34] A. S. Hansen, T. Bhagde, Y. Qian, A. Cavazos, R. M. Huchmala, M. A. Boyer, C. F. Gavin-Hanner, S. J. Klippenstein, A. B. McCoy and M. I. Lester, "Infrared Spectroscopic Signature of a Hydroperoxyalkyl Radical (•QOOH)," J. Chem. Phys. **156**, 014301 (2022).
[35] T. Liu, S. N. Elliott, M. Zou, M. F. Vansco, C. A. Sojdak, C. R. Markus, R. Almeida, K. Au, L. Sheps, D. L. Osborn, F. A. F. Winiberg, C. J. Percival, C. A. Taatjes, R. L. Caravan, S. J. Klippenstein and M. I. Lester, "OH Roaming and Beyond in the Unimolecular Decay of the Methyl-Ethyl-Substituted Criegee Intermediate: Observations and Predictions," J. Am. Chem. Soc. **145**, 19405-19420 (2023).
[36] T. Liu and M. I. Lester, "Roaming in the Unimolecular Decay of syn-Methyl-Substituted Criegee Intermediates," J. Phys. Chem. A **127**, 10817-10827 (2023).
[37] K. T. Kuwata, M. R. Hermes, M. J. Carlson and C. K. Zogg, "Computational Studies of the Isomerization and Hydration Reactions of Acetaldehyde Oxide and Methyl Vinyl Carbonyl Oxide," J. Phys. Chem. A **114**, 9192-9204 (2010).
[38] L. Vereecken, A. Novelli and D. Taraborrelli, "Unimolecular Decay Strongly Limits the Atmospheric Impact of Criegee Intermediates," Phys. Chem. Chem. Phys. **19**, 31599-31612 (2017).

[39] C. T. Yin and K. Takahashi, "How Does Substitution Affect the Unimolecular Reaction Rates of Criegee Intermediates?," Phys. Chem. Chem. Phys. **19**, 12075-12084 (2017).
[40] D. Cremer, E. Kraka and P. G. Szalay, "Decomposition Modes of Dioxirane, Methyldioxirane and Dimethyldioxirane - a CCSD(T), MR-AQCC and DFT Investigation," Chem. Phys. Lett. **292**, 97-109 (1998).
[41] M. T. Nguyen, D. Sengupta, G. Raspoet and L. G. Vanquickenborne, "Theoretical Study of the Thermal Decomposition of Acetic Acid: Decarboxylation Versus Dehydration," J. Phys. Chem. **99**, 11883-11888 (1995).
[42] T. L. Nguyen, R. Winterhalter, G. Moortgat, B. Kanawati, J. Peeters and L. Vereecken, "The Gas-Phase Ozonolysis of β-Caryophyllene ($C_{15}H_{24}$). Part II: A Theoretical Study," Phys. Chem. Chem. Phys. **11**, 4173-4183 (2009).
[43] T. N. Nguyen, R. Putikam and M. C. Lin, "A Novel and Facile Decay Path of Criegee Intermediates by Intramolecular Insertion Reactions via Roaming Transition States," J. Chem. Phys. **142**, 124312 (2015).
[44] J. H. Kroll, N. M. Donahue, V. J. Cee, K. L. Demerjian and J. G. Anderson, "Gas-Phase Ozonolysis of Alkenes: Formation of OH from Anti Carbonyl Oxides," J. Am. Chem. Soc. **124**, 8518-8519 (2002).
[45] C.-Y. Ng, "Vacuum Ultraviolet Spectroscopy and Chemistry by Photoionization and Photoelectron Methods," Annu. Rev. Phys. Chem. **53**, 101-140 (2002).
[46] Y. Matsuda, N. Mikami and A. Fujii, "Vibrational Spectroscopy of Size-Selected Neutral and Cationic Clusters Combined with Vacuum-Ultraviolet One-Photon Ionization Detection," Phys. Chem. Chem. Phys. **11**, 1279-1290 (2009).
[47] H. L. Han, C. Camacho, H. A. Witek and Y. P. Lee, "Infrared Absorption of Methanol Clusters $(CH_3OH)_n$ with n=2-6 Recorded with a Time-of-Flight Mass Spectrometer Using Infrared Depletion and Vacuum-Ultraviolet Ionization," J. Chem. Phys. **134**, 144309 (2011).
[48] Y. J. Hu, J. W. Guan and E. R. Bernstein, "Mass-Selected IR-VUV (118 nm) Spectroscopic Studies of Radicals, Aliphatic Molecules, and Their Clusters," Mass Spectrom. Rev. **32**, 484-501 (2013).
[49] E. Gloaguen, M. Mons, K. Schwing and M. Gerhards, "Neutral Peptides in the Gas Phase: Conformation and Aggregation Issues," Chem. Rev. **120**, 12490-12562 (2020).
[50] M. A. Boyer and A. B. McCoy (2021). "PyVibPTn, a General Package for Vibrational Perturbation Theory," Zenodo. https://doi.org/10.5281/zenodo.5563090
[51] H. H. Nielsen, "The Vibration-Rotation Energies of Polyatomic Molecules," Phys. Rev. **60**, 794-810 (1941).
[52] V. Barone, "Anharmonic Vibrational Properties by a Fully Automated Second-Order Perturbative Approach," J. Chem. Phys. **122**, 014108 (2004).
[53] A. B. McCoy and E. L. Sibert, III, "Perturbative Calculations of Vibrational (J=0) Energy Levels of Linear Molecules in Normal Coordinate Representations," J. Chem. Phys. **95**, 3476-3487 (1991).
[54] E. B. Wilson, J. C. Decius and P. C. Cross, *Molecular Vibrations: the Theory of Infrared and Raman Vibrational Spectra*,(McGraw-Hill, New York :, 1955).
[55] M. Mendolicchio, J. Bloino and V. Barone, "General Perturb-Then-Diagonalize Model for the Vibrational Frequencies and Intensities of Molecules Belonging to Abelian and Non-Abelian Symmetry Groups," J. Chem. Theory Comput. **17**, 4332-4358 (2021).
[56] J. M. L. Martin, T. J. Lee, P. R. Taylor and J. P. François, "The Anharmonic Force Field of Ethylene, C_2H_4, by Means of Accurate Ab Initio Calculations," J. Chem. Phys. **103**, 2589-2602 (1995).
[57] Q. Yang and J. Bloino, "An Effective and Automated Processing of Resonances in Vibrational Perturbation Theory Applied to Spectroscopy," J. Phys. Chem. A **126**, 9276-9302 (2022).
[58] L. A. Curtiss, P. C. Redfern and K. Raghavachari, "Gaussian-4 theory," J. Chem. Phys. **126**, (2007).
[59] M. J. Frisch, G. W. Trucks, H. B. Schlegel, G. E. Scuseria, M. A. Robb, J. R. Cheeseman, G. Scalmani, V. Barone, G. A. Petersson, H. Nakatsuji, X. Li, M. Caricato, A. V. Marenich, J. Bloino, B. G. Janesko, R. Gomperts, B. Mennucci, H. P. Hratchian, J. V. Ortiz, A. F. Izmaylov, J. L. Sonnenberg, Williams, F. Ding, F. Lipparini, F. Egidi, J. Goings, B. Peng, A. Petrone, T. Henderson, D. Ranasinghe, V. G. Zakrzewski, J. Gao, N. Rega, G. Zheng, W. Liang, M. Hada, M. Ehara, K. Toyota, R. Fukuda, J. Hasegawa, M. Ishida, T. Nakajima, Y. Honda, O. Kitao, H. Nakai, T. Vreven, K. Throssell, J. A.

Montgomery Jr., J. E. Peralta, F. Ogliaro, M. J. Bearpark, J. J. Heyd, E. N. Brothers, K. N. Kudin, V. N. Staroverov, T. A. Keith, R. Kobayashi, J. Normand, K. Raghavachari, A. P. Rendell, J. C. Burant, S. S. Iyengar, J. Tomasi, M. Cossi, J. M. Millam, M. Klene, C. Adamo, R. Cammi, J. W. Ochterski, R. L. Martin, K. Morokuma, O. Farkas, J. B. Foresman and D. J. Fox, Gaussian 16, Gaussian, Inc., Wallingford, CT, 2016.

[60] J. M. Beames, F. Liu, M. I. Lester and C. Murray, "Communication: A New Spectroscopic Window on Hydroxyl Radicals Using UV Plus VUV Resonant Ionization," J. Chem. Phys. **134**, 241102 (2011).

[61] J. M. Beames, F. Liu and M. I. Lester, "1+1 ' Resonant Multiphoton Ionisation of OH Radicals via the $A^2\Sigma^+$ State: Insights from Direct Comparison with A-X Laser-Induced Fluorescence Detection," Mol. Phys. **112**, 897-903 (2014).

[62] S. G. Lias, "Ionization Energy Evaluation" in *NIST Chemistry WebBook, NIST Standard Reference Database Number 69*; Linstrom, P. J., Mallard, W. G., Eds.; National Institute of Standards and Technology: Gaithersburg MD, 20899 DOI: 10.18434/T4D303 (retrieved March 18, 2024).

[63] T. L. Liu, M. J. Zou, A. Caracciolo, C. A. Sojdak and M. I. Lester, "Substituent Effects on the Electronic Spectroscopy of Four-Carbon Criegee Intermediates," J. Phys. Chem. A **126**, 6734-6741 (2022).

[64] T. L. Nguyen, L. McCaslin, M. C. McCarthy and J. F. Stanton, "Communication: Thermal unimolecular decomposition of *syn*-CH_3CHOO: A kinetic study," J. Chem. Phys. **145**, 131102 (2016).